

## Enhanced photodegradation of methyl orange with TiO<sub>2</sub> nanoparticles using a triboelectric nanogenerator

This article has been downloaded from IOPscience. Please scroll down to see the full text article.

2013 Nanotechnology 24 295401

(<http://iopscience.iop.org/0957-4484/24/29/295401>)

View [the table of contents for this issue](#), or go to the [journal homepage](#) for more

Download details:

IP Address: 143.215.17.188

The article was downloaded on 28/06/2013 at 01:29

Please note that [terms and conditions apply](#).

# Enhanced photodegradation of methyl orange with TiO<sub>2</sub> nanoparticles using a triboelectric nanogenerator

Yuanjie Su<sup>1,2,4</sup>, Ya Yang<sup>1,4</sup>, Hulin Zhang<sup>1</sup>, Yannan Xie<sup>1</sup>, Zhiming Wu<sup>2</sup>, Yadong Jiang<sup>2</sup>, Naoki Fukata<sup>3</sup>, Yoshio Bando<sup>3</sup> and Zhong Lin Wang<sup>1,3</sup>

<sup>1</sup> School of Materials Science and Engineering, Georgia Institute of Technology, Atlanta, GA 30332-0245, USA

<sup>2</sup> State Key Laboratory of Electronic Thin Films and Integrated Devices, School of Optoelectronic Information, University of Electronic Science and Technology of China (UESTC), Chengdu 610054, People's Republic of China

<sup>3</sup> MANA, International Center for Materials Nanoarchitectonics, National Institute for Materials Science, 1-1 Namiki, Tsukuba, 305-0044, Japan

E-mail: [zlwang@gatech.edu](mailto:zlwang@gatech.edu)

Received 14 April 2013, in final form 21 May 2013

Published 27 June 2013

Online at [stacks.iop.org/Nano/24/295401](http://stacks.iop.org/Nano/24/295401)

## Abstract

Methyl orange (MO) can be degraded by a photocatalytic process using TiO<sub>2</sub> under UV irradiation. The photo-generated holes and electrons can migrate to the surface of TiO<sub>2</sub> particles and serve as redox sources that react with adsorbed reactants, leading to the formation of superoxide radical anions, hydrogen peroxide and hydroxyl radicals involved in the oxidation of dye pollution. Here, we fabricated a polytetrafluoroethylene–Al based triboelectric nanogenerator (TENG) whose electric power output can be used for enhancing the photodegradation of MO with the presence of TiO<sub>2</sub> nanoparticles, because the TENG generated electric field can effectively boost the separation and restrain the recombination of photo-generated electrons and holes. Due to the photoelectrical coupling, the degradation percentages of MO for 120 min with and without TENG assistance are 76% and 27%, respectively. The fabricated TENGs have potential applications in wastewater treatment, water splitting, and pollution degradation.

 Online supplementary data available from [stacks.iop.org/Nano/24/295401/mmedia](http://stacks.iop.org/Nano/24/295401/mmedia)

(Some figures may appear in colour only in the online journal)

## 1. Introduction

Wastewater treatment, pollution degradation and energy shortage are among the most crucial problems that humanity has to solve. Currently, based on piezoelectric [1–3], triboelectric [4, 5], and pyroelectric [6, 7] effects, nanogenerators have been extensively fabricated for applications in driving electronic devices [8, 9], self-powered nanosystems [10–12], and sensors [13–18]. Owing to the enormous distribution and

mobility of water systems in the environment, wastewater treatment and liquid pollutant degradation can be a vital issue for the whole of society [19]. Not only does the wastewater treatment affect human health and hygiene, but also it has a great influence on the entire ecosystem for all creatures. Consequently, a green, energy-saving and low cost method for purifying water sources is desired. In general, wastewater from textile manufacturing, including aromatic compounds and organic dyes, presents a potential hazard to the environment that must be dealt with before the wastewater can be discharged [20]. Titanium dioxide (TiO<sub>2</sub>) is one of

<sup>4</sup> These authors contributed equally to the work.

the most investigated photocatalysts and has been found to be capable of decomposing a wide variety of organics and inorganics in both liquid and gas phases [21]. The basic principle of TiO<sub>2</sub> photocatalysis involves photo-generated electrons and holes migrating to the surface of TiO<sub>2</sub> particles and serving as redox sources that can react with adsorbed reactants, leading to the formation of superoxide radical anions, hydrogen peroxide and hydroxyl radicals. The reactive hydroxyl radical enables oxidation of organic compounds in aqueous solution, mineralizing them to CO<sub>2</sub> and H<sub>2</sub>O. Although TiO<sub>2</sub> photocatalytic degradation is a promising means for degradation of dyes, the low separation efficiency and relatively high recombination of photo-generated carriers limit the quantum efficiency of photodegradation. Here, we demonstrate that the photodegradation of MO can be effectively enhanced by using a triboelectric nanogenerator (TEMG). The TEMG was fabricated by using polytetrafluoroethylene (PTFE) and an Al layer as the triboelectric materials to harvest the mechanical energy based on the triboelectric effect [22, 23]. By converting mechanical energy into electricity, the TEMG yields an electric field in the MO solution to promote the separation and inhibit the recombination of photo-generated electrons and holes for the photocatalytic oxidation of dye pollutants.

## 2. Experimental details

TiO<sub>2</sub> nanopowders (Anatase, Evonik) were sonicated using Branson Transonic 2510 and placed in the reactor. Methyl orange (SIGMA-ALDRICH, ACS reagent, dye content 85%) was placed in the reaction vessel and the mixture was placed at the same position all the time for the UV irradiation and absorption measurement. With plenty of deionized water filled in the reaction vessel, the concentration of TiO<sub>2</sub> is 0.6 g l<sup>-1</sup> and the concentration of MO is 20 mg l<sup>-1</sup>. Prior to irradiation, the solution was stirred in the dark at a speed of 6000 rev min<sup>-1</sup> for 20 min. The methyl orange (MO) was irradiated with a solar simulator (500 W model 91160, Newport) with an AM 1.5 spectrum distribution (100 mW cm<sup>-2</sup>). In this work, the photocatalytic degradation of MO using TiO<sub>2</sub> nanoparticle was conducted without O<sub>2</sub> bubbling. Every 30 min during the photodegradation process, a small amount of MO suspension was taken out and then stirred for 10 min in order to precipitate the particles in solution. Subsequently, the absorption spectra of MO were measured using a UV-visible spectrophotometer (JASCO V-630).

The morphology and nanostructure of TiO<sub>2</sub> particles were characterized using a LEO 1530 field emission scanning electron microscope (SEM) operated at 10 kV and a transmission electron microscope (TEM) TF30 operated at 300 kV. Phase identification of TiO<sub>2</sub> was conducted by means of x-ray diffraction (XRD) using a PANalytical X'Pert PRO diffractometer.

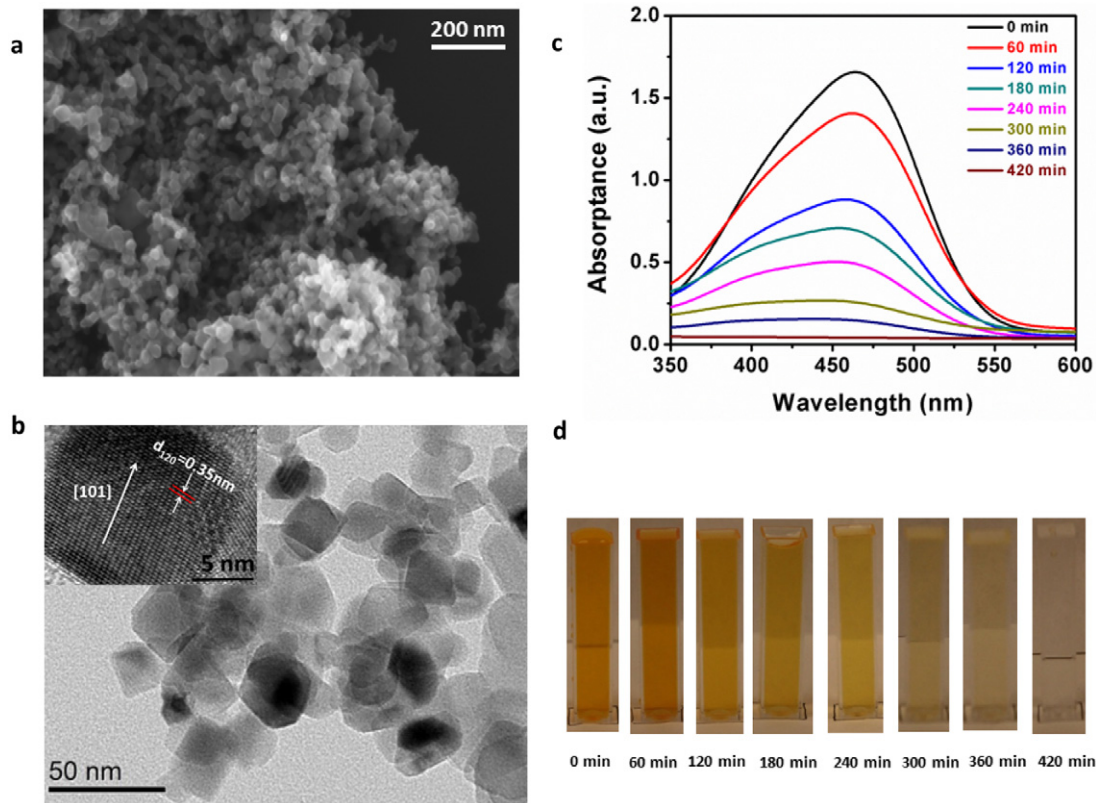
The TEMG consists of polyethylene terephthalate (PET) film, a Cu film, a PTFE film, and an Al foil, where PET film was selected for the substrates at the top and bottom of the TEMG. PTFE film serves as the contact layer. Cu film acts as

the back electrode of PTFE. The layer of Al plays dual roles of electrode and triboelectric materials. The Al foil and Cu film was pasted on the PET substrates to protect the generator from mechanical impact. The microstructure of the TEMG layer was characterized by scanning electron microscopy (SEM) as shown in figure S3 (available at [stacks.iop.org/Nano/24/295401/mmedia](http://stacks.iop.org/Nano/24/295401/mmedia)). Figure S3(a) (available at [stacks.iop.org/Nano/24/295401/mmedia](http://stacks.iop.org/Nano/24/295401/mmedia)) demonstrates Al foil to be the electrode layer. Figures S3(b) and (c) (available at [stacks.iop.org/Nano/24/295401/mmedia](http://stacks.iop.org/Nano/24/295401/mmedia)) shows the PTFE film layer and the Cu foil, respectively. Figure S3(d) (available at [stacks.iop.org/Nano/24/295401/mmedia](http://stacks.iop.org/Nano/24/295401/mmedia)) illustrates the Cu foil under PTFE as one electrode for conducting the inductive charges. According to figure S3 (available at [stacks.iop.org/Nano/24/295401/mmedia](http://stacks.iop.org/Nano/24/295401/mmedia)), the thicknesses of Al foil, Cu film and PTFE film are about 96.5 μm, 171.3 μm, 30.2 μm, respectively. The PET was from DURA with a thickness of 220 nm. The contact electrode (Al) and back electrode (Cu) of the TEMG were connected to the Pt electrodes in MO solution in order to produce an electric field. In addition, the Pt electrodes were covered by polydimethylsiloxane (PDMS) film to prevent the current conduction in MO solution. The TEMG was mechanically triggered by a linear motor that provided dynamic impact with controlled speed, force and frequency. A rectifying bridge was connected to the TEMG to convert the alternating current (AC) to direct current signals. The output performance of the TEMG was measured using Stanford Research Systems. SR560 and SR570 low noise current amplifiers were used to record voltage and current, respectively.

## 3. Results and discussion

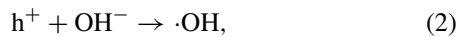
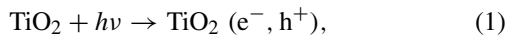
Figure 1(a) shows a scanning electron microscopy (SEM) image of TiO<sub>2</sub> nanoparticles, indicating that the diameter of the particles ranges from 20 to 40 nm. As displayed in figure S1 (available at [stacks.iop.org/Nano/24/295401/mmedia](http://stacks.iop.org/Nano/24/295401/mmedia)), an x-ray diffraction (XRD) pattern of TiO<sub>2</sub> illustrates a dominance of the anatase over the rutile form in a ratio of 6:1. The phase and crystal structure of the TiO<sub>2</sub> particles were confirmed by the lattice TEM image in figure 1(b). The high magnification TEM image in the inset of figure 1(b) demonstrates that the distance between lattice fringes is 0.35 nm, which can be attributed to (101) of the anatase TiO<sub>2</sub> phase.

Figure 1(c) reveals absorption spectra of MO decomposed in the presence of TiO<sub>2</sub> photocatalyst under UV irradiation. The spectrum ranges from 350 to 600 nm with a peak at the wavelength of 464 nm. It can be seen that the characteristic absorption peak intensity of MO decreases with increasing degradation time. After 420 min of UV irradiation, the degradation of MO is up to 97% and the absorption peak is totally removed. Figure 1(d) displays the decoloration of MO suspension at different degradation times. The color change from dark orange to colorless indicates that the MO has been degraded by the TiO<sub>2</sub> nanoparticles under UV irradiation. The mechanism of the photodegradation of MO by using TiO<sub>2</sub>



**Figure 1.** (a) SEM image of TiO<sub>2</sub> nanoparticles. (b) TEM image of the TiO<sub>2</sub> nanoparticles. Inset: high magnification TEM for the lattice image of TiO<sub>2</sub>. (c) Absorption spectra of MO degraded by TiO<sub>2</sub> under UV irradiation. (d) Decoloration of MO at different photodegradation times.

nanoparticles is proposed as follows [24]:



dye + O<sub>2</sub><sup>·-</sup> or ·OH → peroxyated or hydroxylated intermediates → degraded products.

UV irradiation of TiO<sub>2</sub> excites electrons from a filled valence band to an empty conduction band, giving rise to electron–hole pairs. The valence band holes (h<sup>+</sup>) can migrate to surfaces of TiO<sub>2</sub> particles and react with adsorbed OH<sup>-</sup> to produce hydroxyl radicals (·OH), whereas the conduction band electrons (e<sup>-</sup>) migrate to the surfaces and react with adsorbed electron acceptors, such as O<sub>2</sub>. Although TiO<sub>2</sub> photocatalysis is an attractive approach for decomposing the organic compounds and dye pollution, there are some factors that restrain the performance of photodegradation, such as separation rate, migration of photo-generated carriers, and recombination. The low migration speed of photo-generated holes and electrons, poor separate efficiency, and relatively high recombination rate suppress the quantum efficiency of TiO<sub>2</sub> photocatalytic degradation. In order to solve this problem, we use the TENG to yield an electric field in the solution of MO so as to accelerate the separation and migration of photo-generated carriers and inhibit their recombination. Figure 2(a) indicates a schematic diagram of

the system for degradation of MO by photocatalytic oxidation. The TENG is connected to Pt electrodes in MO solution to form parallel built-in electric field. The rectifying bridge circuit was used to convert the ac output into dc. UV light source was placed 10 cm above the level of MO. Due to the insulating property of the contacting material, the triboelectric charges stored in a single layer can be retained for hours or even days [25]. Therefore, the fabricated TENG photocatalysis system can work with high performance for several years at least. Figure 2(b) shows a schematic diagram of the TENG. In this study, the TENG was made of PET, a Cu layer, PTFE film, and Al foil. PET was selected as the material for substrates owing to its flexibility, light weight, and low cost. PTFE is the triboelectric contact layer. The Cu layer between the PET substrate and contact layer of PTFE acts as a back electrode. The layer of Al plays dual roles of electrode and contact surface. The working mechanism of the TENG is based on the triboelectric effect [5]. When PTFE is in contact with the aluminum layer, electrons are transferred from Al into PTFE due to the different triboelectric coefficients. Once the two surfaces are separated, the electric potential difference is produced, leading to an open-circuit voltage [26]. The output voltage can be given by

$$V_{\text{oc}} = \frac{\sigma d}{\epsilon_0} \quad (4)$$

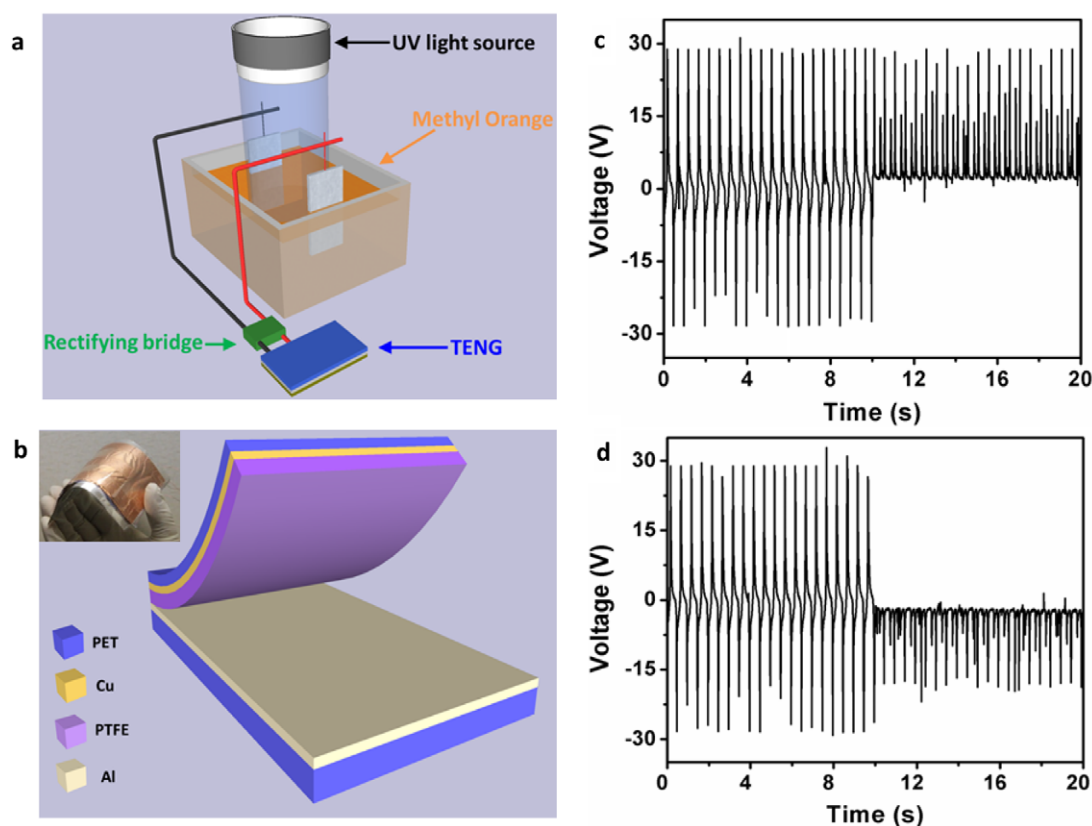


**Figure 2.** (a) Schematic diagram of TENG assisted photodegradation of MO. (b) Schematic diagram of the fabricated triboelectric nanogenerator (TENG). Inset: photograph of a fabricated TENG. (c) Open-circuit voltage of the TENG with forward connection. (d) Open-circuit voltage of the TENG with reverse connection.

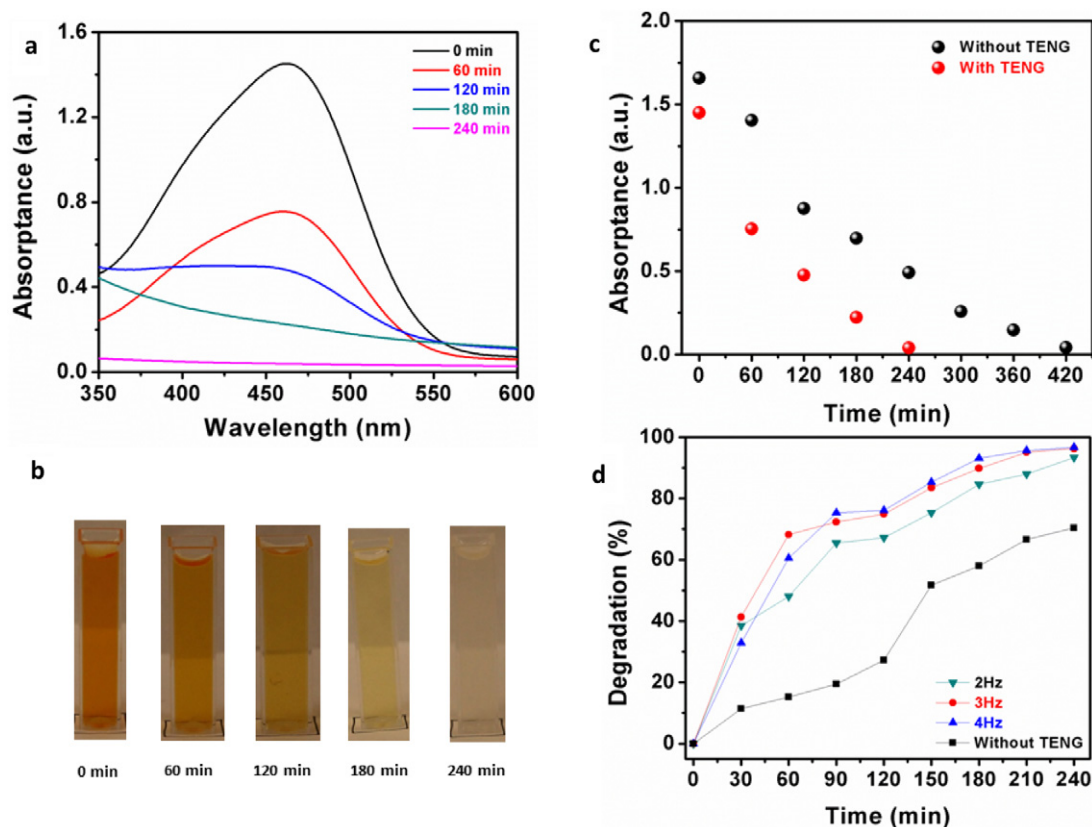
where  $\sigma$  is the triboelectric charge density,  $\epsilon_0$  is the vacuum permittivity, and  $d$  is the distance between two contacting surfaces. According to equation (4), an AC open-circuit voltage is achieved by periodic separation and contact between the PTFE and Al films, which was triggered by a mechanical press. Parts (c) and (d) of figure 2 show the output performance of the fabricated TENG under the forward and reversed connections, where the output voltage is up to 30 V. The left part in figures 2(c) and (d) is the output of the TENG without a rectifying bridge circuit while the right part is the output rectified by a rectifying bridge circuit. Owing to the insulation of the PDMS film covered on the Pt electrodes, no current was detected in the MO solution. The MO decomposition is based on the  $\text{TiO}_2$  photocatalytic process rather than conduction of current between electrodes, which is the main factor in electrocatalytic degradation.

Figure 3(a) illustrates the absorption spectrum of MO photodegradation with  $\text{TiO}_2$  under the electric field triggered by the TENG. The characteristic absorption peak decreases with increasing degradation time. With the assistance of the TENG, the characteristic absorption peak of MO goes down more quickly than the one without the TENG assistance. The decoloration in figure 3(b) displays color changing of the MO solution during the photocatalysis process, indicating that the TENG assisted photodegradation can be finished in only 240 min, which is almost half the time for the one without TENG assistance. Figure 3(c) shows the value of

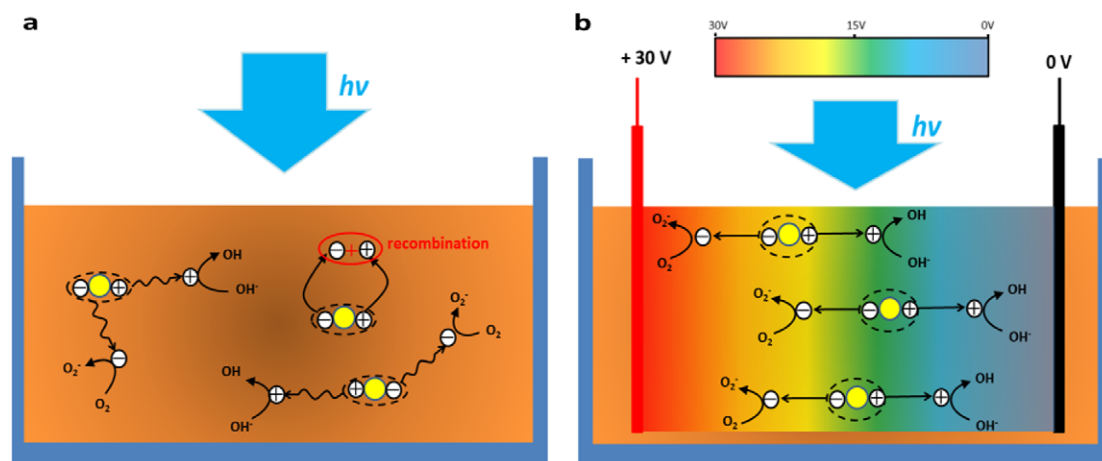
the absorption peak at 464 nm under different degradation times, indicating that the TENG does boost the speed of photodegradation of MO and shorten the duration required for completely mineralizing the dye.

Figure 3(d) illustrates the photodegradation rate of MO assisted by the TENG under different frequencies. The TENG was driven by a linear motor that provides mechanical impact with controlled frequency. According to figure 3(d), the degradation rate is proportional to the output frequency of the TENG and all the degradation percentages assisted by the TENG are much higher than that without the assistance of the TENG at the same time. The voltage peak value and pulse shape under the different frequencies were found to be almost the same in figure S2 (available at [stacks.iop.org/Nano/24/295401/mmedia](http://stacks.iop.org/Nano/24/295401/mmedia)); more voltage peaks in a unit time period means higher effective voltage, that can give rise to a stronger effective electric field intensity. The electric field in the MO solution not only accelerates the migration and the separation of photo-generated carriers, but also restrains recombination. A larger electric field will push more holes towards adsorbed  $\text{OH}^-$  and thus produce more hydroxyl radicals ( $\cdot\text{OH}$ ) for the degradation reaction with MO. In consequence, the speed of photodegradation is increased with increasing output frequency of the TENG.

The mechanism for the TENG enhancing the photocatalytic degradation of MO is demonstrated in figure 4. Part (a)



**Figure 3.** (a) Absorption spectra of MO in photodegradation assisted by the TENG. (b) Decoloration of MO at different photodegradation times. (c) Plot of the absorption peak at 464 nm versus the photodegradation time. (d) Plot of the degradation percentage versus the time under the frequencies of 2, 3, and 4 Hz with a control without TENG assistance.



**Figure 4.** (a) Mechanism of the TiO<sub>2</sub> photocatalytic degradation of MO under UV irradiation. (b) Mechanism of the TiO<sub>2</sub> photocatalytic degradation of MO under UV irradiation assisted by the TENG.

and (b) of figure 4 are cross-section views for the photodegradation of MO without and with TENG assistance respectively. As revealed in figure 4(a), photo-generated holes and electrons cannot react with OH<sup>-</sup> and O<sub>2</sub> until they migrate to the surface of TiO<sub>2</sub> particles where these reactants are adsorbed. Furthermore, the photo-excited electrons and holes on the surface of TiO<sub>2</sub> cannot separate immediately when they are created, having the probability of recombination. However,

once the electric field was generated in MO by the TENG in figure 4(b), the photo-generated electrons and holes were driven to separate at once and flow in opposite directions by the electric force, which can increase the rate of separation of electron-hole pairs and inhibit the recombination. Moreover, instead of migration, the photo-excited carriers were pushed towards the surface of TiO<sub>2</sub> or even directly to adsorbed OH<sup>-</sup> and O<sub>2</sub> for oxidation, which can increase the speed

of degradation reaction significantly. This is a novel method for enhancing separation and suppressing the recombination of photo-generated carriers by an electric field generated by the triboelectric effect. Since mechanical movement is very common in our daily life, this approach provides an effective and easy way to address wastewater treatment and liquid pollution almost everywhere. Furthermore, by increasing the size of the TENG for energy harvesting, a larger scale of pollution degradation could also be possible.

#### 4. Conclusion

We have demonstrated the enhanced photodegradation of methyl orange as driven by a triboelectric nanogenerator. By converting the mechanical energy into electric output, the TENG yields an electric field in the MO solution, boosting the separation and migration of photo-generated carriers on the surface of TiO<sub>2</sub>, leading to suppression of the recombination. Consequently, with the assistance of the TENG the degradation rate was promoted considerably, shortening the degradation time from 420 to 240 min. At the photodegradation time of 120 min, the degradation with and without TENG assistance has the values 76% and 27%, respectively. The fabricated TENGs have potential applications in the field of wastewater treatment, water splitting and pollution degradation.

#### Acknowledgments

This work was supported by the US Airforce, MURI, US Department of Energy, Office of Basic Energy Sciences (DE-FG02-07ER46394), NSF, and MANA, the World Premier International Research Center Initiative (WPI Initiative), MEXT, Japan. Y J Su, Z M Wu, and Y D Jiang acknowledge the support of the National Science Foundation of China via grant No. 61101029. Y J Su also would like to acknowledge a fellowship from the China Scholarship Council (CSC) and the assistance of Y Ding with the transmission electron microscopy.

#### References

- [1] Wang Z L and Song J H 2006 *Science* **312** 242–6
- [2] Wang X D, Song J H, Liu J and Wang Z L 2007 *Science* **316** 102–5
- [3] Lee S, Hong J I, Xu C, Lee M, Kim D, Lin L, Hwang W and Wang Z L 2012 *Adv. Mater.* **24** 4398–402
- [4] Pelrine R, Kornbluh R D, Eckerle J, Jeuck P, Oh S and Pei Q 2001 *Proc. SPIE* **4329** 148–56
- [5] Fan F R, Tian Z Q and Wang Z L 2012 *Nano Energy* **1** 328–34
- [6] Yang Y, Guo W, Pradel K C, Zhu G, Zhou Y, Zhang Y, Hu Y, Lin L and Wang Z L 2012 *Nano Lett.* **12** 2833–8
- [7] Yang Y, Jung J H, Yun B K, Zhang F, Pradel K C, Guo W and Wang Z L 2012 *Adv. Mater.* **24** 5357–62
- [8] Hu Y, Lin L, Zhang Y and Wang Z L 2011 *Adv. Mater.* **24** 110–4
- [9] Zhu G, Yang R, Wang S and Wang Z L 2010 *Nano Lett.* **10** 3151–5
- [10] Wang Z L and Wu W 2012 *Angew. Chem.* **51** 11700–21
- [11] Wang Z L 2008 *Sci. Am.* **298** 82–7
- [12] Wang Z L 2011 *Adv. Mater.* **24** 279–84
- [13] Beeby S P, Tudor M J and White N M 2006 *Meas. Sci. Technol.* **17** 175–95
- [14] Roundy S, Steingart D, Frechette L, Wright P and Rabaey J 2004 *Lect. Notes Comput. Sci.* **2920** 1–17
- [15] Yang Y, Lin L, Zhang Y, Jing Q S, Hou T C and Wang Z L 2012 *ACS Nano* **6** 10378–83
- [16] Pan C F, Yu R M, Niu S M, Zhu G and Wang Z L 2013 *ACS Nano* **7** 1803–10
- [17] Lee M, Bae J, Lee J, Lee C S, Hong S and Wang Z L 2011 *Energy Environ. Sci.* **4** 3359–63
- [18] Lin L, Hu Y, Xu C, Zhang Y, Wen X and Wang Z L 2013 *Nano Energy* **2** 75–81
- [19] Wang Z L 2011 *Adv. Mater.* **24** 280–5
- [20] Yang Y, Zhang H L, Lee S, Kim D, Hwang W and Wang Z L 2013 *Nano Lett.* **13** 803–8
- [21] Siham A Q and Salman R S 2002 *J. Photochem. Photobiol. A* **148** 161–8
- [22] Zhu G, Pan C F, Guo W X, Chen C Y, Zhou Y S, Yu R M and Wang Z L 2012 *Nano Lett.* **12** 4960–5
- [23] Zhu G, Lin Z H, Jing Q S, Bai P, Pan C F, Yang Ya, Zhou Y S and Wang Z L 2013 *Nano Lett.* **13** 847–53
- [24] Tias P, Penney L M and Timothy J S 2007 *Environ. Sci. Technol.* **41** 4720–7
- [25] Saurenbach F, Wollmann D, Terris B D and Diaz A F 1992 *Langmuir* **8** 1199–203
- [26] Nemeth E, Albrecht V, Schubert G and Simon F 2003 *J. Electrostat.* **58** 3–16